

Low cycle fatigue damage mechanism of the lightweight alloy Al2024

S. Khan^a, F. Wilde^b, F. Beckmann^b, J. Mosler^{a,*}

^a Helmholtz-Zentrum Geesthacht, Institute of Materials Research, Materials Mechanics, Max-Planck-Str. 1, 21502 Geesthacht, Germany

^b Helmholtz-Zentrum Geesthacht, Institute of Materials Research, Structural Research on New Materials, Max-Planck-Str. 1, 21502 Geesthacht, Germany

ARTICLE INFO

Article history:

Received 6 April 2011

Received in revised form 3 November 2011

Accepted 20 November 2011

Available online 2 December 2011

Keywords:

Low cycle fatigue

Micro-tomography

Aluminum alloys

Quasi-brittle damage

ABSTRACT

Detection of cracks in Al2024 T351 specimens subjected to low cycle fatigue loading by a certain non-destructive inspection technique is demonstrated. In the experimental phase of the study, notched round specimens were fatigue loaded. The tests were performed at different constant strain amplitudes at room temperature. For identifying the crack initiation loci, the specimens were removed from the testing machine after a certain number of cycles and were non-destructively inspected via X-ray technique. Pictures were taken successively while incrementally turning the sample. The re-constructed data were visualized via software (VGStudio MAX 2.1) to obtain a 3D image of the specimen, showing all the details of its inner structure. By taking "virtual" slices from the data, quantification of microstructural properties was done using classical methods. This allowed verifying some frequently mentioned statements concerning the low cycle fatigue behavior of high-strength aluminum alloys. Furthermore, new findings related to the tri-axiality dependence on the resulting fracture process and those related to damage initiation caused by decohesion were also discovered.

© 2011 Elsevier Ltd. All rights reserved.

1. Introduction

Engineering components and structures may be subjected to cyclic loading resulting in plastic flow. Such plastic deformation and its respective accumulation with cycles is a major cause of damage that, eventually, lead to material failure. Damage is related to the irreversible processes at the materials microstructure. Therefore, it affects the material constitutive response at meso/macroscale as well. From a physical point of view, damage, defined as the appearance of new surfaces in a material, can be decomposed into three stages: initiation, growth and coalescence. It has been shown [1] that damage initiates preferentially at special sites, such as heterogeneous inclusions. Different initiation mechanisms have been observed: inclusion rupture [2], inclusion/matrix decohesion [3] or matrix cracking around the inclusions in the case of fatigue of metals. In the low cycle fatigue (LCF) regime, accumulative microstructural changes take place in the form of persistent slip bands, rearrangement of dislocation systems into cell structures, void nucleation and growth at the secondary phase inclusions [4,5]. The latter mechanism corresponds to high strain amplitudes, for which very short lifetimes are usually expected. Regardless of the loading conditions, the early estimation of cracks is essential for preventing failure of the considered structure.

For elucidating the aforementioned phenomena and processes, analyzing the internal structure in mechanical components is thus

of much importance. In the present paper, focus is on lightweight and high-strength aluminum alloys. However, by conventional techniques, such as laboratory X-ray and ultrasonic imaging, the size and shape of subsurface non-metallic inclusions and cracks defining the fatigue behavior of this alloy cannot be detected (the maximum resolution is typically 100 μm). Recently, micro-tomography using the synchrotron radiation has been utilized for evaluating the physical or chemical properties of materials with extremely high sensitivity. Typical properties are the density, the underlying chemical elements, the chemical bonding and the microstructure.

Certainly, the aforementioned material characterization is relatively time-consuming and its efficiency can be improved by accompanying modeling. Furthermore, modeling provides often the only way for a more detailed quantitative analysis. In this context, micromechanics is a powerful framework for the investigation and prediction of materials behavior at the meso/macroscale incorporating characteristics of the respective microstructure. However, for using such models, the progressive degradation in the material caused by damage accumulation has to be known – qualitatively as well as quantitatively. In summary, modeling without a previous material characterization is not reasonable.

Since conventional techniques cannot be used for detecting most of the relevant micromechanical features in high-strength aluminum alloys such as Al2024, other testing methods have to be used. In this connection, synchrotron radiation based micro-tomography (SRμCT) allows for artifact free investigations showing not only a high spatial resolution but also a high density resolution

* Corresponding author.

E-mail address: joern.mosler@hzg.de (J. Mosler).

in the reconstructed volume [6]. This is due to the high intensity and the low divergence of the monochromatized synchrotron radiation. SR μ CT has been applied to 3D measurement and in situ observation of fatigue crack propagation [7]. The used beamline HARWI II operated by Helmholtz-Zentrum Geesthacht at the storage ring DORIS III of Deutsches Elektronen-Synchrotron (DESY), Hamburg, Germany, enables SR μ CT with a high spatial resolution down to less than 3–4 μm and is obtained by measuring the modulation transfer function (MTF) of a densified edge in the projection [8].

Within our investigations, focus is on monotonic loading and low cyclic fatigue (LCF) of the aluminum alloy Al2024. For that purpose, round notched bars with different radii taken from 100 mm thick sheet are examined. The specimens have been extracted from the short-transverse direction. In the present study, the SR μ CT is applied to the 3D measurement of interfaces and inclusions causing fatigue crack in that alloy. This paper is divided into five sections. Initially, the choice of the characterization method is justified and the material specification is described. Subsequently, a microstructural characterization is given. Finally, the experimental and tomography set-up is briefly discussed. The paper is completed by a discussion and a conclusion.

2. Why Synchrotron micro-tomography?

An essential aspect is the choice of the experimental methods and the hardware. Several direct and non-direct experimental methods for measuring damage accumulation have been developed (electrical resistance, acoustic emission, infrared thermography, hardness measurement, destructive and non-destructive tomography, etc.). Most of them are based on analyzing side effects associated with damage processes. Clearly, direct measurement methods show several advantages compared to their aforementioned indirect counterparts. Thus, only direct methods are considered within this research work.

Synchrotron radiation based X-ray micro-tomography (SR μ CT) has emerged during the last decade as a new powerful direct technique to visualize the interior of an untransparent sample at the microscale, cf. [9,10]. The subsequent argumentation explains the choice of SR μ CT:

- The physical phenomenon ranges between different scales, e.g. microscale (particles) and nano-scale (damage). Thus, techniques like transmission electron microscopy (TEM) or focused ion beam (FIB) destructive tomography are too detailed and metallographic destructive methods or even more sophisticated methods like neutron tomography are too general.
- The heterogeneous microstructure and the limited number of experiments require special non-destructive techniques like tomography.
- SR μ CT data allow analyzing damage effects (defects, interfaces such as cracks) combined with the microstructural properties (matrix and inclusions) and their interaction.
- SR μ CT possesses higher resolution compared to alternative X-ray tomography (e.g. μ -focus tube) [11] and high density resolution too. Furthermore, it provides the necessary monochromatic beam intensity to apply μ CT on high absorbing samples without beam-hardening artifacts.

Traditional methods (optical and scanning electron microscopy) have become the common tools for investigating crack growth behavior in materials. These methods provide important 2D information about fracture processes. However, fracture in the interior differs from that at the surface, even if the material is homogeneous. Thus, fracture is intrinsically a 3D phenomenon.

For instance, if a crack appears stagnant on the surface, it may have grown for a significant distance in the internal.

Although synchrotron micro-tomography shows a lot of advantages, the method is not without problems. More explicitly, tomographic images often contain different kinds of artifacts. The so-called *ring artifacts* are very common (formation of concentric rings in the images around the center of rotation of the tomographic set-up, see Fig. 14). They are caused by differences in the individual pixel response of the detector or by impurities on the scintillator crystals. They occur in lab based tomography as well, since they are independent of the X-ray source. A way to reduce such artifacts is the shape and size filtering during the post-processing of the images. In summary, such problems associated with synchrotron micro-tomography can be overcome by experienced researchers.

3. Material specification

Al2024-T351 is an aluminum alloy known due to its good mechanical properties, damage tolerance and resistance against corrosion. Therefore it has been used for decades in aircraft applications, especially in fuselage skins. The material under investigation was supplied in form of a rolled sheet in a T351 temper (solution heat treated, air-quenched, stress-relieved). The chemical composition is given in the Table 1.

The strong anisotropy of the microstructure, caused by the manufacturing process, influences the failure strain significantly.

Table 1
Chemical composition (wt.%) of Al2024 T351, [12].

Cu	Mg	Mn	Si	Fe	Cr	Al
4.11	1.12	0.46	0.048	0.05	0.003	Rest

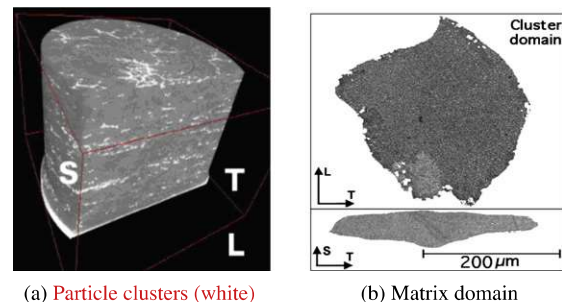


Fig. 1. SR μ CT analysis on a 100 mm thick plate (S-direction) of virgin Al2024, [13].

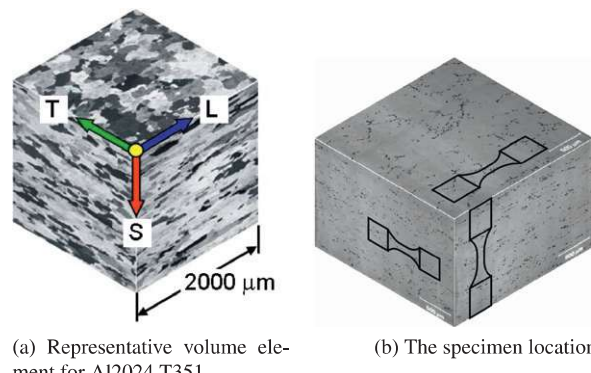


Fig. 2. Microstructure of a 100 mm thick plate of Al2024 – optical microscope.

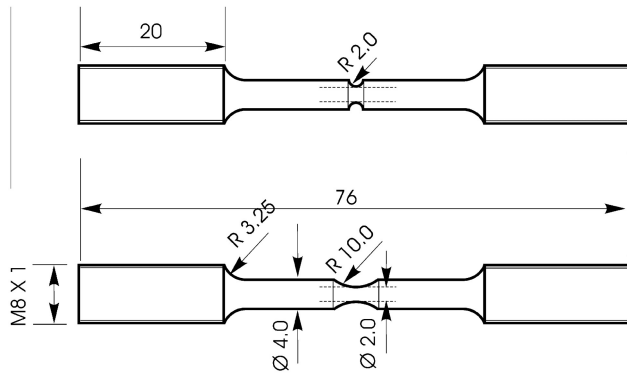
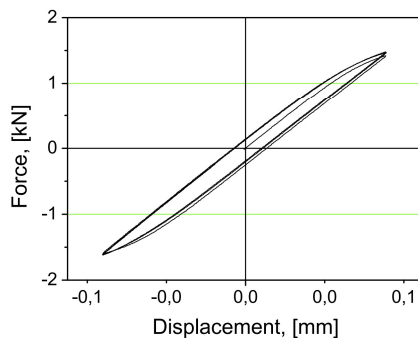


Fig. 3. The specimens' geometry.

Consequently, the loading direction is very important. The microstructure of Al2024 has already been studied extensively using optical microscopy, scanning electron microscopy and SR μ CT [12,13]. Fig. 1a shows a reconstructed view of the investigated volume. The particle clusters appear white, while the surrounding matrix is gray. The particles are aligned in a network-like structure (clusters) which separates the matrix into domains. These domains have “pancake” shape, with the S-direction (thickness direction) as the shortest axis and almost identical dimensions in L- and T-directions (longitudinal and transversal directions respectively), see Fig. 1b. The largest particles in the microstructure (clusters) have high copper concentration and have the equivalent diameter $23.5 \pm 16.7 \mu\text{m}$ (diameter of a sphere having the same volume).

4. Experimental procedures

Round notched bar (Fig. 3) specimens having 2 and 10 mm notch radius were manufactured (thickness direction) from a 100 mm thick plate (Fig. 2b). To avoid the influence of surface roughness on the nucleation of cracks, the specimens have been carefully polished mechanically before testing. Both tests (monotonic and cyclic) were performed enforcing a displacement controlled loading condition (Fig. 8a). The testing parameters for cyclic loadings remain confined to symmetric loading amplitudes (asymmetry of cycle $R = -1$) and frequency 0.01 Hz. A typical measured load-elongation graph is given in Fig. 4a. These particular tests were stopped with the progression of the maximum load, see Fig. 4b. The minimal cross-section of the specimens was reduced up to 2 mm (Fig. 3) for achieving better absorption resolution. The geometry was modified to localize damage in the middle part of the specimens keeping a quasi-homogeneous stress



(a) Force elongation curve

state along the minimum cross-section (hour-glass specimen). The variation of the stress state (tri-axiality) has been achieved by introducing notches.

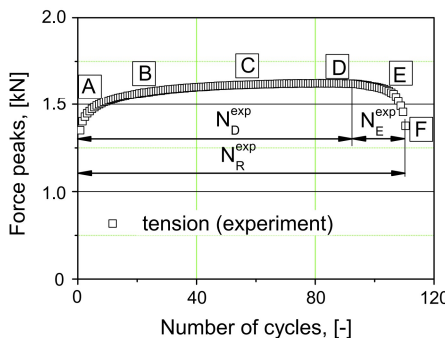
Determining the onset of damage initiation and further evolution is the main purpose of this work. Specimens of both geometries have been tested till marker stages (Fig. 4b) classified as:

- A. This stage serves as a reference. It was reported in earlier works that rupture of the brittle particles takes already place during this stage (Fig. 5a, cf. [14]).
- B. During this stage, the specimen hardens and significant plasticity can be observed.
- C. A state of saturation is achieved, the stress remains constant. This stage represents the major portion of the specimen's fatigue life. Damage on the microscale already initiates during this stage (Fig. 5b).
- D. This point indicates the onset of the decrease in force. It corresponds to micro-cracks propagating into meso-cracks. The meso-crack initiation loci are significant in lifetime assessment.
- E. Various meso-cracks cumulate and constitute a large fatal propagating macrocrack.
- F. Final failure.

The total fatigue lifetime of a structure can be additively decomposed into cycles required for damage initiation (N_D) and final rupture (N_R). For a sound design, N_D usually takes up the major part of the lifetime with N_E representing the time required for macrocrack evolution. At point D (Fig. 4b) the specimens degrade and soften mainly due to the formation of voids and cracks. However, at the microscale damage initiates significantly earlier – already in the saturation region C. Although that has been known for several decades, there is a lack of an experiment proof. Thus, synchrotron micro-tomography seems to be promising. Clearly, in situ measurements are possible in principle. However, overweight of the machine and vibrations involved could possibly distort the results (discussed in Section 8). For this reason, a staggered approach has been used. More precisely, a single experiment was considered first, till the respective specimen broke. Subsequently, different specimens (same material orientation and geometry) were tested till the stages defined in Fig. 4b. Finally, these specimens were characterized.

5. Fractographic characterization

Fig. 6 reveals the fractured surfaces of the round notched bars after total failure. For evaluating the shape and profile of the fracture surfaces, stereogram analysis were carried out with 3D image



(b) Tensile force peaks and definition of different damage stages (A-F)

Fig. 4. Cyclic mechanical response of small notched round bars of Al2024 (see Fig. 3).

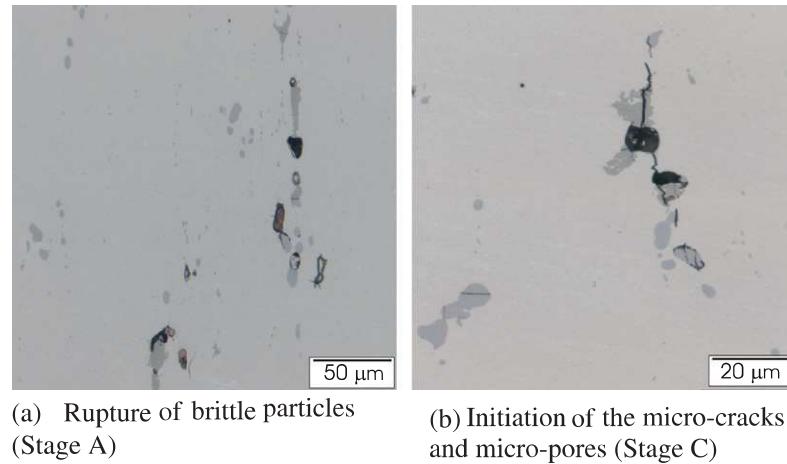


Fig. 5. Different damage stages visualized using an optical microscope (cut lateral view).

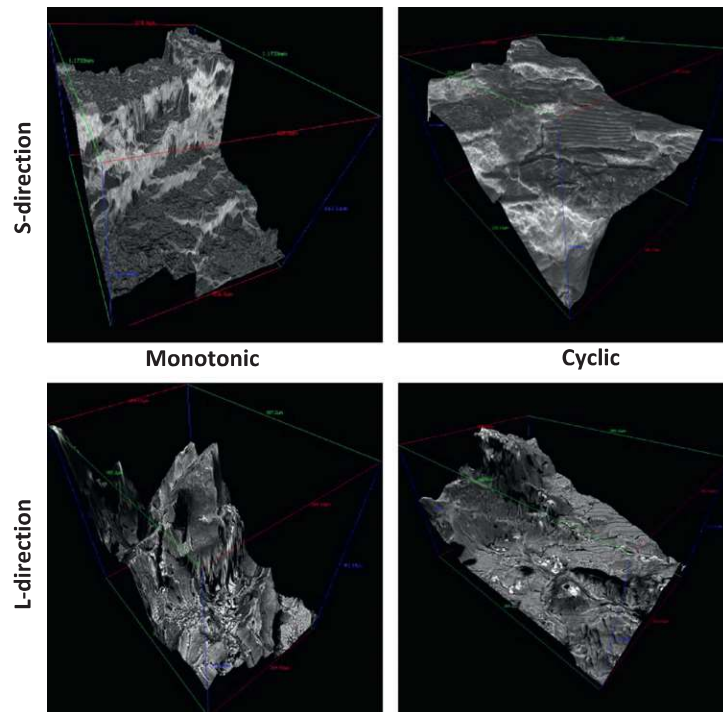


Fig. 6. Fractured surface profiles of Al2024-T351 in L- and T-direction (SEM data, visualized using 3D image re-construction software, Mex (AliconaTM, Inc.) [15]).

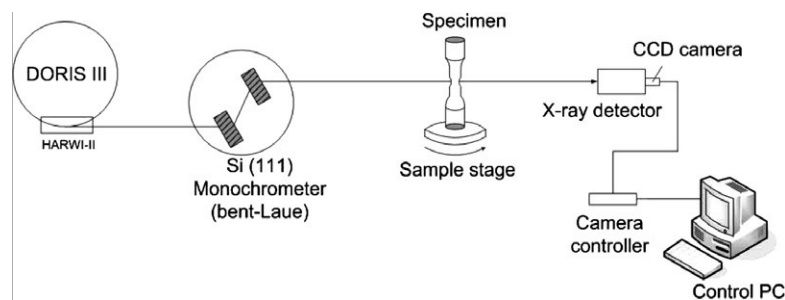


Fig. 7. Schematic illustration of the synchrotron micro-tomography measurement system.

re-construction software, Mex (AliconaTM, Inc.) [15]. The images have been re-constructed from SEM data (scanning electron microscope). The stereogram was obtained by tilting $\pm 5^\circ$ from the top. It

can be seen that the monotonic and cyclic fracture of the specimen extracted from the thickness direction (S) consists of sharp bright planes, characteristic of brittle fracture, whereas the L-direction

Table 2Parameters of SR μ CT at beamline HARWI-II.

	HARWI II
Photon energy	25–30 keV
Pixel size in projection	2.21 μ m
Measured spatial resolution in projection	3.42 μ m
Voxel size in reconstruction	4.42 μ m
Reconstructed volume	6.76 mm \times 6.76 mm \times 4.87 mm

Table 3Components used for SR μ CT.

CCD camera	Finger lake instruments PLO9000, 3056 \times 3056 pixels, pixel size: 12 μ m 16 bit digitalization at 10 MHz
Optical lens	Camera lens; Nikon Inc., 35 mm focal length
Fluorescent screen	CdWO ₄ single crystal, thickness 590 μ m

reveals a dimple structure associated with ductile deformation. The reason for such a direction-dependent fracture mechanism is the formation of particle clusters aligned in the rolling direction, forming internal networks separating the structure into flat disks of Al-matrix domains surrounded by particle free bands (PFB). The interesting fracture behavior in the S (thickness) direction led to a more detailed study using SR μ CT.

6. Tomography set-up

X-ray imaging was carried out at HARWI-II beamline operated by HZG at the storage ring DORIS III of DESY, the largest synchrotron radiation facility in Germany. The schematic illustration of the measurement is shown in Fig. 7. The samples were set approximately 40 m from the X-ray source and they have been fixed on a rotational stage without pre-tensioning. The zooming tube with the fluorescent screen and a cooled CCD camera were employed as a detector. As discussed previously, the specimen thickness was chosen to be small in order to lower the X-ray attenuation and thus to enhance both the spatial and the density resolution of the tomogram [8]. The beamline parameters and the components used for all scans are given in Tables 2 and 3 respectively.

Based on the penetration depth, the energy of the incident beam was chosen to be 25 keV, and the micro-tomography images of the sample were observed. The sample is located as close as possible to the fluorescent screen (2–4 mm). The CCD detector was located a bit further away (25 cm). For 3D reconstruction, a set of 900 radiographs of the sample was recorded over 180° rotations, where each rotation was 0.2°. The size of the voxels in the reconstructed images was 4.42 μ m. Image slices were reconstructed from the series of projections based on a filtered back projection algorithm [16]. For the visualization of the re-constructed voxel data and volumetric analysis, VGStudio MAX 2.1 was later used.

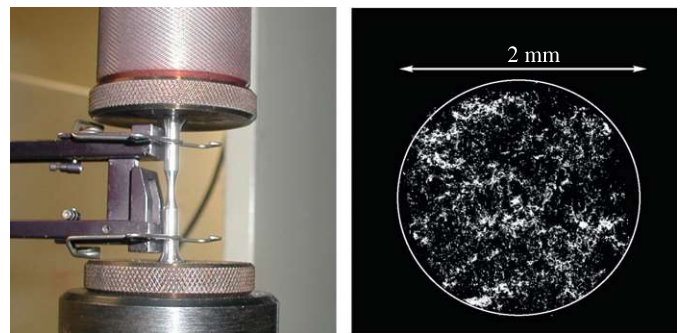
7. Results and discussion

The reconstructed 3D rendering of the unloaded microstructure of the present material is shown in Fig. 1. The network structure with Cu particles belongs to Al–Cu eutectic phase (EU), while the large cell-shaped regions surrounded by the EU phase belong to primary α phase dendrite cells.

7.1. Uniaxial tests

Fig. 8b shows a typical 2D cross-sectional (top view) image from the re-constructed tomography data set (uniaxial tensile loading¹).

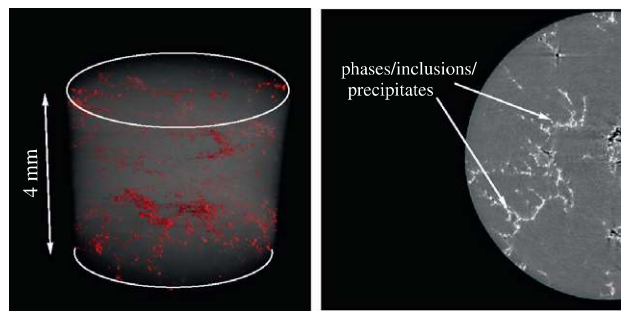
¹ In the figure, only an hourglass specimen is shown, but the same set-up was also used for 2 mm and 10 mm notched specimen.



(a) Test set-up for the hourglass specimens

(b) Slice of the reconstructed SR μ CT measurements, middle section of the hourglass specimen (tensile loading)

Fig. 8. Loading device (HZG testing hall) and visualization of the SR μ CT experiments (beamline HARWI-II).



(a) 3D rendering of the specimen's interior showing micropores originating from the particle/matrix interface

(b) An example of a 2D reconstructed slice close to the middle section of the specimen

Fig. 9. Re-construction of the hourglass specimen (Uniaxial tensile loading), see Fig. 8a with SR μ CT.

A complex crack morphology can be seen at the center of the image, with relatively spherical micropores (black) and complex intermetallic particle groups (white) in the surrounding matrix, cf. Fig. 9b. White particles are heterogeneous inclusions or precipitates of Al₂Cu and Al₂CuMg secondary phases. They appear white due to different absorption related to copper. In Fig. 8b, the cluster network of these inclusions is evident (white layer). During monotonic loading a decohesion takes place between these particles and the matrix resulting in void formation (several black dots appear on the gray background). The debonding is only observed at these clusters.

Fig. 9a shows a 3D re-construction of the specimen with 4 mm scanning height. Damage is scattered all over the volume and has the same pattern as the particle layers which indicates that decohesion has been the underlying mechanism (red spots are voxels with a high contrast, i.e. damage). SR μ CT investigations on monotonically loaded specimens (loaded up to different levels of plastic deformation close to the failure point) were a trial attempt to judge and check the capability of the tomography setup with respect to the resolution.

7.2. LCF tests

Earlier studies [14] on cyclically deformed notched specimens (4 mm radius) of the same alloy indicated that the crack front is neither a straight line nor does it lie in the symmetry plane of

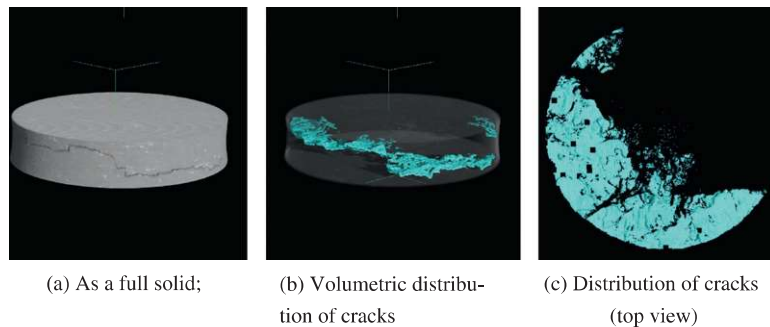


Fig. 10. Re-constructed SR μ CT data; 3D images of the notched specimen ($r = 4$ mm), specimen lasted for 154 cycles.

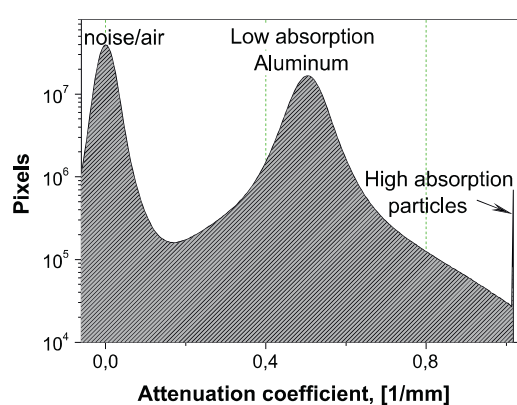


Fig. 11. Attenuation coefficient measured by using SR μ CT. From left to right, the gray values of the different constituents are displayed, i.e. noise/air, matrix material, heterogeneous inclusions/particles.

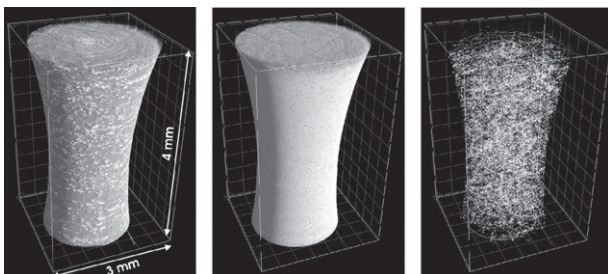


Fig. 12. Results of the SR μ CT: 10 mm notched round bar specimen (undeformed virgin specimen).

Table 4
Volumetric analysis of Al2024.

Specimen (mm)	Voxels, ROI (average)	Total volume (excl. noise) (mm ³)	Volume (high density objects) (mm ³)
2	4.1e8	16.6	0.1115
10	3.92e8	15.7	0.1563

the specimen cf. Fig. 10. However, those specimens were deformed till the appearance of surface cracks and hence, the experiments gave no information on the initiation of damage and lacked a comparison with the uniaxial tensile loading state.

In Fig. 11, the number of voxels has been plotted against the considered attenuation coefficient for specimens failing under

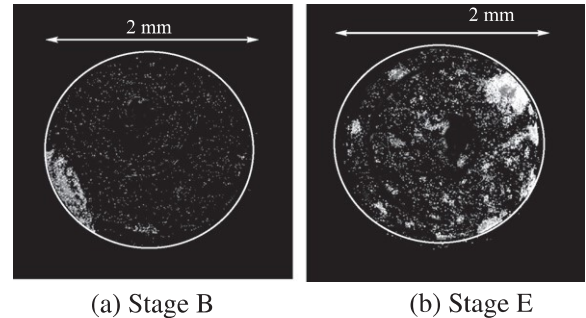


Fig. 13. Results of the SR μ CT for cyclic loading conditions: Top views of the damage in 10 mm notched specimen at different stages (94 and 105 cycles, respectively).

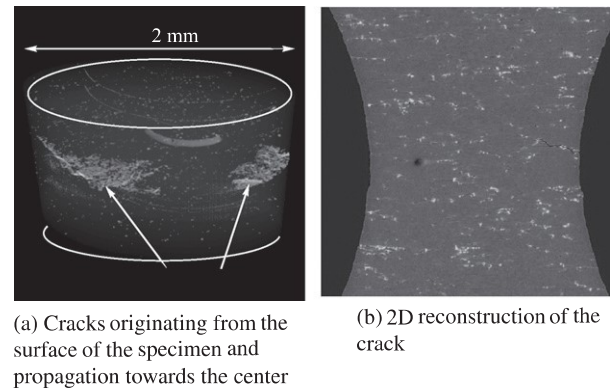


Fig. 14. Results of the SR μ CT: Cyclically loaded hourglass specimens, lasting for 143 cycles.

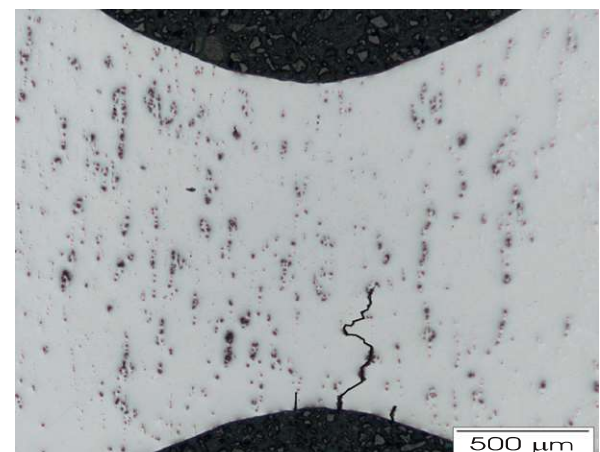


Fig. 15. Results of an optical microscopy study: 10 mm notched specimen at stage E, longitudinally cut and polished afterwards.

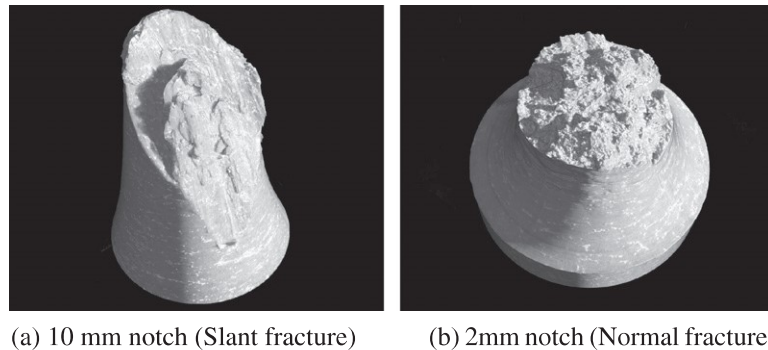


Fig. 16. Results of the SR μ CT: Fractured surfaces.

fatigue loading. Three areas can be distinguished based on the absorption level. Air which surrounds the specimen, as shown by a bounding box (see Fig. 12) and noise in the system appear on the left of the histogram. Cracks are discontinuities in the material filled with air and thus indistinguishable from the surrounding air. Aluminum being the matrix material comes next followed by high density heavy copper particles. The composition in terms of voxels is given in Table 4. In all cases, a specific region of interest (ROI, Fig. 12) is extracted which excludes noise and other experimental tolerances.

The volumetric analysis shows an unusually high volume of particles at the middle of the plate, the site which forms the notches of the specimen. Among the particles, damage initiates from the bigger ones located near the notch root for cyclic loading and at the middle of the specimen for monotonic loading.

Cracks already nucleate during the hardening stage (stage B, Fig. 4b). Fig. 13a shows a small micro-crack initiating from the surface of the 10 mm notch specimen and the high density particles distributed all over the volume. Subsequently, during the saturation and degradation stage (stage D and E, Fig. 4b), multiple cracks near the surface evolve (large particles; Fig. 13b) and merge into a major surface crack resulting eventually in the total failure. A similar observation has been noted for 2 mm notches. However, a single crack dominates the failure process in this case. The vacant dark rings (Fig. 13) near the edge appear black due to the removal of the artifacts during post-processing.

Fig. 14 shows cracks in the interior of the specimen. Accordingly, their propagation is very complex and shows a wavy path. After the tomography, some specimens have been longitudinally (destructive imaging) cut and the mid-plane has been examined using an optical microscope, cf. Fig. 15. In the particular case of the 10 mm specimen at stage E, two cracks in addition to the primary crack have formed at the surface (81 and 63 μ m length, respectively). The primary crack connects various clusters of particles and has a length of 752 μ m. The resulting fracture surfaces of the 2 mm as well as for the 10 mm notch specimen, now generated by the SR μ CT data, are shown in Fig. 16. Numerous subsurface cracks can be seen under the fracture surface for the 10 mm notch specimen, whereas no such cracks were detected for the 2 mm notch specimen.

8. Concluding remarks

In the present work, the high resolution synchrotron X-ray micro-tomography has been demonstrated to be a promising method for visualizing and analyzing fatigue damage in a high strength aluminum alloy. This technique provides much more information than traditional methods. More explicitly and in contrast to conventional measuring techniques, the synchrotron X-ray

micro-tomography allows to analyze specimens non-destructively and equally importantly, to measure the volumetric fully 3D distribution of micro-defects. Such information is of utmost importance for understanding the underlying physical processes and thus, it is required for developing physically sound constitutive models.

By using the aforementioned measuring technique, the frequently postulated statement that a macroscopic crack forms at the surface in case of fatigue, while it starts propagating in the interior for monotonic loading could be verified for the high-strength aluminum alloy Al2024. However and besides this commonly accepted fact, several additional new findings associated with low cycle fatigue could be also reported. Although some of those have already been conjectured earlier based on post-mortem analysis, cf. [14], their final correctness could only been verified by the presented synchrotron micro-tomography measurements.

In addition to the already conjectured statements, the reported tri-axiality dependence on the failure process is completely new. More explicitly, the 2 mm and 10 mm notched specimens have different fracture mechanisms. While the crack originates from different particles at the notch root for lower tri-axiality (10 mm notch), a single straight crack initiating from the surface and eventually, resulting in fatal failure has been observed for the 2 mm notched specimen. Equally important, decohesion of particles is the major source driving damage accumulation during the first loading stages. Such insights allow developing physically sound constitutive models.

The new SR μ CT systems at the Helmholtz-Zentrum Geesthacht beamlines IBL and HEMS at the 3rd generation SR-facility PETRA-III of DESY will further improve the spatial resolution of the measuring method with the speed greatly enhanced due to much higher photon flux. Combining these new facilities with an in situ mechanical device will allow analyzing the micro-defects in the full tension phase. By doing so, more detailed information concerning the failure process is expected.

Acknowledgements

The authors express their gratitude to the staff at HASYLAB (DESY) Hamburg for their support regarding the late night shifts. Furthermore, the support by A. Vyshnevskyy (ex-HZG) and D. Hellmann (HZG, Geesthacht) is gratefully acknowledged.

References

- [1] Sarkar J, Kutty T, Conlon K, Wilkinson D, Embury J, Lloyd D. Tensile and bending properties of aa5754 aluminum alloys. Mater Sci Eng a-Struct Mater Propert Microstruct Process 2001;52:316.
- [2] Llorca J, Martin A, Ruiz J, Elices M. Particulate fracture during deformation of a spray formed metal-matrix composite. Metall Trans a-Phys Metall Mater Sci 1993;24:1575.

- [3] Dierickx P, Verdu C, Reynaud A, Fougeres R. A study of physico-chemical mechanisms responsible for damage of heat treated and as-cast ferritic spheroidal graphite cast irons. *Scripta Materialia* 1996;34:261.
- [4] Klesnil M. Fatigue of metallic materials. Elsevier Science Publishers; 1980.
- [5] Polak J. Cyclic plasticity and low cycle fatigue life of metals. Elsevier Science Publishers; 1991.
- [6] Beckmann F. Neutron and synchrotron-radiation based imaging for applications in materials science – from macro to nanotomography. Weinheim: Wiley VCH Verlag; 2008 [Ch. 7].
- [7] Müller B, Pfrunder F, Chiocca L, Ruse N, Beckmann F. Visualising complex morphology of fatigue cracks in voxel based 3d datasets. *Mater Sci Technol* 2006;22:1038–44.
- [8] Beckmann F, Donath T, Fischer T, Dose J, Lippmann T, Lottermoser L, et al. New developments for synchrotron-radiation-based microtomography at desy. Tech. rep., DESY (Proc SPIE 6318:631810–631811); 2006.
- [9] Morgeneyer T, Starink M, Sinclair I. Evolution of voids during ductile crack propagation in an aluminium alloy sheet toughness test studied by synchrotron radiation computed tomography. *Acta Materialia* 2008;56:1671.
- [10] Proudhon H, Buffiere J, Fouvy S. Three-dimensional study of a fretting crack using synchrotron X-ray micro-tomography. *Eng Fract Mech* 2007;74:782.
- [11] Bernhardt R, Müller B, Theruner P, Schliephake H, Wyss P, Beckmann F, et al. Comparison of microfocus – and synchrotron X-ray tomography for the analysis of osteointegration around Ti6Al4V-implants. *Euro Cells Mater* 2004;7:42.
- [12] Quan G, Heerens J, Brocks W. Distribution characteristics of constituent particles in thick plate of 2024Al-T351. *Prakt Metallogr* 2004;41:304.
- [13] Steglich D, Brocks W, Pardoent T. Anisotropic ductile fracture of Al2024 alloys. *Eng Fract Mech* 2008;75:3692–706.
- [14] Khan S, Vyshevskyy JMA, Mosler J. Low cycle lifetime assessment of Al2024 alloy. *Int J Fatigue* 2010;32:1270–7.
- [15] Alicona I. Mex-Alicona imaging solutions. Graz-Austria; 2000–2009.
- [16] Kak A, Slaney M. Principles of computerized tomographic imaging. New York: IEEE Press; 1988.